IEEE Access
Multidisciplinary | Rapid Review | Open Access Journal

Received March 30, 2020, accepted April 22, 2020, date of publication April 29, 2020, date of current version May 18, 2020.

Digital Object Identifier 10.1109/ACCESS.2020.2991206

Design of Galvanic Coupling Intra-Body Communication Transceiver Using Direct Sequence Spread Spectrum Technology

W. K. CHEN[1,2], Z. L. WEI[1,2], Y. M. GAO[1,2], Ž. LUČEV VASIĆ[3], (Member, IEEE), M. CIFREK[3], (Member, IEEE), M. I. VAI[2,4,5], (Senior Member, IEEE), M. DU[1,6], AND S. H. PUN[5]

[1]College of Physics and Information Engineering, Fuzhou University, Fuzhou 350116, China
[2]Key Laboratory of Medical Instrumentation and Pharmaceutical Technology of Fujian Province, Fuzhou 350116, China
[3]Faculty of Electrical Engineering and Computing, University of Zagreb, 10000 Zagreb, Croatia
[4]Department of Electrical and Computer Engineering, Faculty of Science and Technology, University of Macau, Macao 999078, China
[5]State Key Laboratory of Analog and Mixed-Signal VLSI, University of Macau, Macau 999078, China
[6]Key Laboratory of Eco-Industrial Green Technology of Fujian Province, Wuyi University, Nanping 354300, China

Corresponding author: Y. M. Gao (fzugym@gmail.com)

This work was supported in part by the National Natural Science Foundation of China under Grant U1505251, in part by the Project of Chinese Ministry of Science and Technology under Grant 2016YFE0122700, and in part by the Project of S&T Department of Fujian Province under Grant 2018I0011.

ABSTRACT Intra-body communication (IBC) uses the human body as the transmission medium for electrical signals, and it features the following advantages: low power consumption, strong anti-interference ability, high data security, and broad application scenarios. However, some technical issues still need to be addresses, such as the choice of the best modulation and demodulation scheme in different application scenarios, influence of human activity on IBC performance, variable signal-to-noise ratio (SNR), and influence of transmission distance change on different modulation and demodulation methods. This paper adopts direct sequence spread spectrum (DSSS) communication and phase modulation to realize DSSS-differential phase shift keying (DPSK) and DPSK modulation transmission of baseband data. Moreover, the Costas loop method is employed to achieve reliable symbol recovery. Under the same conditions, in vivo experiments were conducted to compare the performance of DSSS-DPSK and DPSK galvanic coupling IBC transceivers. Notably, these transceivers are affected by the changes in SNR, transmission distance, and human activities. Results show that the bit error rate (BER) of the DPSK scheme is 40 times larger than the DSSS-DPSK scheme in a 30 cm channel length and different SNR experiments. When the BER performance changes from extremely poor (1.40×10^{-1}) to excellent (1.51×10^{-6}), the SNR of DSSS-DPSK scheme only needs to be improved by 16 dB. In contrast, when the BER performance changes from extremely poor (1.54×10^{-1}) to good (1.65×10^{-5}), the SNR of DPSK scheme needs to be improved by 25 dB. With a SNR of -5 dB, the BER ratios of the DPSK scheme is 7 times larger than the DSSS-DPSK scheme. Also, DSSS-DPSK scheme is more sensitive to changes in motion status than DPSK.

INDEX TERMS Intra-body communication, galvanic coupling, IBC transceiver, bit error rate, direct sequence spread spectrum (DSSS).

I. INTRODUCTION

Intra-body communication (IBC) technology uses the human body as an electrical signal transmission medium for establishing communication [1], [2]. IBC has the following characteristics: extremely low power consumption, no antenna design and frequency band limitation, low radiation, and transmission range limited to the human body. IBC is an effective method to realize information transmission between various wearable or implantable medical sensors on the human body surface, as well as around and inside the body [3], and to establish Medical Body Area Networks (MBANs) [4], [5]. In IBC, a pair of transmitting electrodes is used to inject a safe alternating current into the body

The associate editor coordinating the review of this manuscript and approving it for publication was Venkata Rajesh Pamula.

surface. The coupling electrical signals are transmitted within the human body [6], [7]. The receiving electrodes collect differential signals in other parts of the human body. The galvanic coupling technique has better adaptability and stability than other types of IBC because the information transmission process occurs completely on the human body and is not easy affected by external influences [8]. This coupling type has a body surface in vivo communication ability, making it an important branch of IBC [9]–[11].

Research on galvanic coupling IBC mainly focuses on the establishment of human models and channel characteristics experiments [10]–[13]. There are few reports on the comparison of performances among galvanic coupling IBC transceivers. In a previous study [13] a quasi-static field electromagnetic model of galvanic coupling IBC including capacitive effects was established. In addition, the transmission characteristics of coupling current in human body were studied. A galvanic coupling IBC transceiver with continuous-phase frequency shift keying (2CPFSK) signal modulation and non-coherent demodulation was designed on the FPGA platform. Many galvanic coupling IBC transceivers are similar to that in [13]. In a previous study [14], a simple IBC transceiver was designed using two programmable system-on-chips (PSoC). In [15], a frequency selective digital transmission (FSDT) method was employed to design a set of transmitting and receiving devices for multi-channel electric acupuncture. In [16], modulated data current was introduced into the human body through an electrode that monitors implanted artificial heart. In [17], a binary frequency shift keying (BFSK) receiver and an on-off keying (OOK) transmitter were used to form an IBC system for fall prevention monitoring. In a previous research [18] the energy consumption and data rate of several IBC transceiver systems was compared. The above-mentioned reports [13]–[18] did not compare the performance of galvanic coupling IBC transceivers employing different modulation methods under the same conditions (i.e., test environment, test equipment, experimental settings, and similar peripheral circuits). In [19], two galvanic coupling IBC transceivers employing BPSK and QPSK were compared under the same conditions, but the authors did not draw relevant conclusions for different modulation and demodulation methods under different SNR conditions and channel lengths.

Research on the effects of changes in SNR, transmission distance, and human activity under the same conditions while using different modulation methods for IBC are limited [20], which restricts the development of IBC technology and its application. Therefore, a comprehensive reference for the selection of modulation and demodulation method in different application scenarios of IBC technology is needed.

The galvanic coupling IBC transceiver designed in this paper is based on direct sequence spread spectrum (DSSS) technology. Because of its reliable transmission at a low SNR and strong security performance, it is widely used in military, mobile communications, satellite communications and other fields. IBC transceiver pays great attention to the reliability and confidentiality in practical applications. Good anti-noise performance can resist the effects of human activities, low-frequency bioelectricity, and channel length changes, as well as improve the IBC system's reliability. Strong confidentiality can improve the security of IBC [21]. Since DSSS can meet the above requirements, we adopt the DSSS-DPSK scheme to design the IBC transceiver to improve the performance of the IBC transceiver.

This design uses field programmable gate array (FPGA, XC6SLX16) as a platform, which adopts DSSS communication and phase modulation to realize the DSSS-differential phase shift keying (DPSK) and DPSK modulation transmission of baseband data, respectively. To improve anti-noise performance, accurately extract bit synchronization signals, and to achieve reliable symbol recovery, a Costas loop is used. Two kinds of transceivers are equipped with the same peripheral circuit used to realize the current holding of signal transmission and receiving signal pre-processing. Finally, in vivo experiments are conducted under the same conditions to compare the performance of DSSS-DPSK and DPSK galvanic coupling IBC transceiver systems. This study includes an analysis of the influence of changes in SNR, transmission distance, and human activity, making the conclusions credible and effective.

II. METHODS

A. MODULATION METHOD SELECTION

Digital signal transmission methods are divided into baseband transmission and bandpass transmission. Digital baseband signals are generally suitable for transmission in short-range wired channels with low-pass characteristics. According to previous reports on the characteristics of galvanic coupling IBC channels, human body channels do not belong to low-pass characteristic channels [22], [23]. Therefore, baseband transmission signals are not suitable for galvanic coupling IBC. For digital signals to be transmitted effectively via human body channels, the baseband signals need to be converted into bandpass signals.

Three basic digital modulation methods are amplitude shift keying (ASK), frequency shift keying (FSK), and phase-shift keying (PSK). In case the 2ASK system is used, the best decision threshold would be half of the input amplitude of the received signal. Given that the channel characteristics of the human body are greatly affected by human positions and movements, decision threshold should be able to adapt dynamically. This is achieved either by restricting human activity or to using highly complicated hardware design. Therefore, being highly sensitive to changes in channel characteristics, ASK method is not suitable for human body channel transmission. The analysis of the anti-noise performance of 2FSK and 2DPSK coherent demodulation directly applies the conclusions in reference [24]: for the same SNR, the bit error rate (BER) of DPSK is always lower than the SNR of the equivalent FSK. For this reason, in this paper an optimized DPSK modulation was chosen for realization of

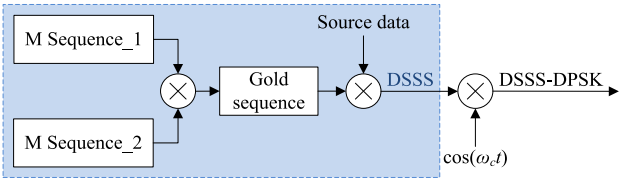

FIGURE 1. Schematic of DSSS-DPSK modulation method.

intra-body communication, namely direct sequence spread spectrum (DSSS) DPSK.

The basic principle of DSSS-DPSK modulation method is shown in Fig. 1. The DSSS-DPSK modulated signal is first subjected to a spread spectrum operation. Subsequently, the spread-spectrum data are subjected to DPSK modulation to obtain a DSSS-DPSK modulated signal. The average power of the DSSS-DPSK signal is equal to the unspread DPSK signal power. The power spectrum shapes of the two devices are basically the same, so the power spectral density of the DSSS signal is 1/N of the unspread signal [21]. Here, N is the ratio of the spread spectrum signal bandwidth to the unspread spectrum signal bandwidth, which is called the spreading coefficient or spreading gain. When N is large, the power spectral density of the DSSS signal can even be lower than the power spectral density of the internal noise of the receiver. In addition, the spectrum of the direct spread spectrum signal has no clearly distinguishable peak component; thus, fraudulent capture of this signal is difficult [21], which provides better security.Anti-noise performance is analyzed as follows. Reference [21] suggests that DSSS-DPSK signal has the same anti-noise performance as DPSK signal when the interference is additive noise. The DSSS-DPSK system has stronger anti-narrowband interference ability, anti-multi-access interference ability, and anti-multipath interference ability than the DPSK system. The above conclusions show that DSSS-DPSK has better anti-noise performance than DPSK modulation but at the cost of occupying a larger channel bandwidth. Good anti-noise performance can resist the effects of human activities, low-frequency bioelectricity, and channel length changes, as well as improve the IBC system's reliability.

B. TRANSMISSION RATE SELECTION

A large spreading sequence N leads to improved anti-noise performance and enhanced security performance [21]. However, for the constant carrier rate, a large N results in low baseband data rate. Using high-frequency IBC signals part of the signal radiates into the air, which increases the risk of data security [25]. Therefore, considering the anti-noise performance and desired data rate, the selected carrier frequency in this paper is 2 MHz, spreading coefficient is $N = 31$, and baseband signal rate is 50 kbps. In practical applications, the above parameters can be modified according to requirements. For comparison with DSSS-DPSK signal transmission, the carrier frequency of 2 MHz is also employed in DPSK, and the baseband signal rate is 1 Mbps.

C. FPGA DESIGN OF THE TRANSMITTER

The transmitter is composed of a source module, a direct digital synthesis (DDS) module, a spread spectrum module, and a DPSK modulation module, as in Fig. 2. To maintain versatility, the source module is designed to directly generate a set of 8-bit "0" and "1" data as the source. The DDS module uses the characteristics of the sine wave phase linearity to realize the design; it includes frequency divider, phase address accumulation module, and phase-to-waveform module. Various design methods of the pseudo-random sequence generator, which is similar to DDS, are available. One approach is to use a pseudo-random sequence value previously written in ROM, and the other is to use multiple cyclic structures and linear shift registers for determination of the module of the pseudo-random sequence generator. In order to increase versatility of the designed spread spectrum module and flexibly set the initial value and parameters of the pseudo-random sequence polynomial, in this work a linear shift register method is adopted. To overcome the BPSK phase ambiguity problem, this design adds a differential coding module before BPSK modulation to implement DPSK modulation. To improve useful power efficiency and prevent inter-symbol interference, the sideband signal spectrum of the transmitted signal is filtered. The original baseband signal is shaped and filtered before modulation. The shaped and filtered signal and DDS module are input into the multiplier to realize DPSK modulation. The DSSS-DPSK signal is sent to the DAC (digital-to-analog converter) and then to the buffer. Finally, the signal is sent to the human body for transmission via transmitter signal and ground electrodes.

D. FPGA DESIGN OF THE RECEIVER

The overall design of the DSSS-DPSK signal receiver is shown in Fig. 3. The main parts of the receiver are an analog front end (AFE), a DPSK demodulation module, a despreading module, and a synchronization module. The analog front end mainly preprocesses the signal that enters the receiver.

In reverse from modulation procedure in Fig. 1, for demodulation of the received DSSS-DPSK signal firstly a DPSK demodulation should be performed, followed by signal despreading to recover the original signal. The coherent demodulation method with optimized BER performance based on the Costas loop method was selected, Fig. 4(a) [26]. Adding a despreading step to the Costas loop results in a DSSS-DPSK demodulator used in this paper, as shown in Fig. 4(b). To realize despreading operation, in our design the low pass filter (LPF) is replaced by two integrate and dump filters (I&DF). I&DF is a decimation low-pass filtering structure without a multiplier, suitable for application in digital software receivers. Costas loop based DSSS-DPSK demodulation completes the demodulation operation while achieving carrier synchronization. Aside from carrier synchronization, pseudo-code sequence synchronization is also required in this study.

In a spread-spectrum communication system, the receiver needs to generate a local pseudo-random code that is the

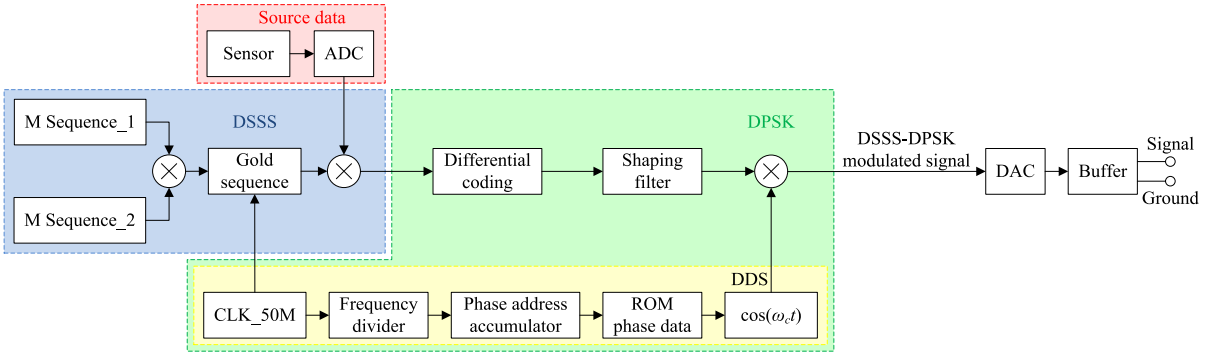

FIGURE 2. Block diagram of DSSS-DPSK transmitter.

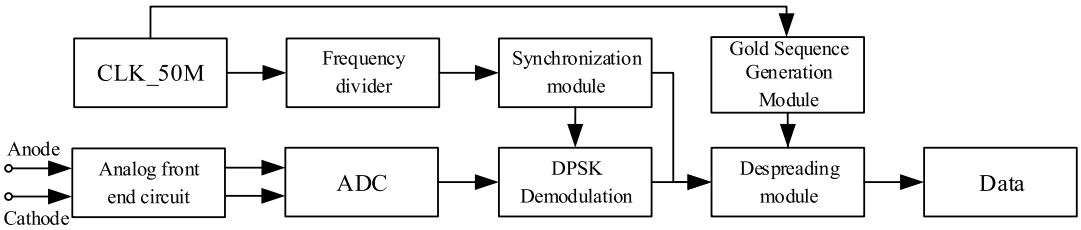

FIGURE 3. Block diagram of the receiver.

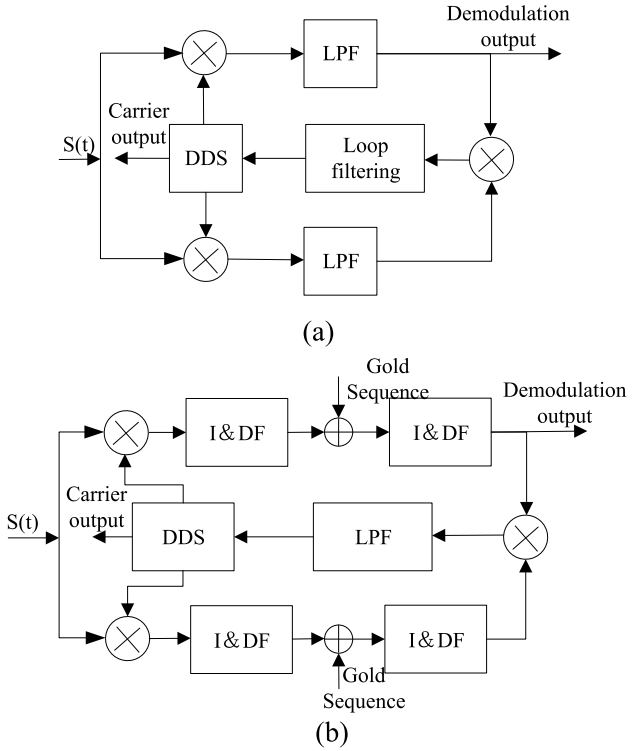

FIGURE 4. Block diagram of (a) Costas loop method and (b) DSSS-DPSK demodulation based on Costas loop.

same and strictly synchronized with the transmitter for despreading. Two steps are needed to capture the local pseudo-random code with the received pseudo-random code at the receiver. The first step is acquisition, that is, to achieve rough synchronization between the two codes, with a phase error lower than one symbol. The second step is tracking, which minimizes phase errors and keeps track. The common acquisition methods are serial search, parallel search, and matched filter acquisition. This design adopts the serial search method, which is stable and consumes less FPGA resources. The principle block diagram of the serial search method is shown in Fig. 5 [20]. The core of this method is to send the output of the IF filter to the detector for integration processing. This method aims to judge whether the integration result is greater than the energy detection threshold, to determine whether useful signals can be captured or not.

In this paper, a phase-locked tracking loop is used to further reduce and maintain the phase difference between the local pseudo-code sequence and the transmitted pseudo-code sequence. The block diagram of the delay-locked tracking loop is shown in Fig. 6. The aim of this method is to use the value of the loop filter output as the control voltage to control the voltage-controlled oscillator frequency. If the pseudo-code phase of the received signal increases, then the voltage-controlled oscillator (VCO) frequency will increase. Otherwise, the frequency of the VCO will decrease.

E. ANALOG FRONT END DESIGN

The receiver analog front end (AFE) is an important part of the communication transceiver. The quality of the analog front end directly affects the receiver performance. The AFE is composed of a filtering module and an amplifier module. In the communication system that uses the human body as a channel, a multi-order filter with high rectangular

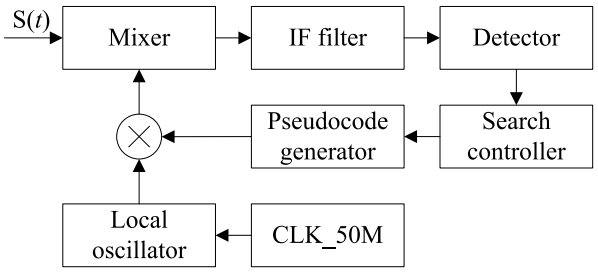

FIGURE 5. Block diagram of serial search method.

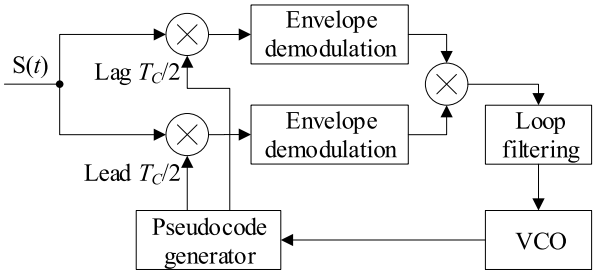

FIGURE 6. Delay phase-locked tracking loop schematic.

coefficient is necessary to improve the performance of the receiving system. This improvement is needed to suppress the high-frequency electromagnetic interference in the surrounding environment and the low-frequency bioelectric interferences, such as ECG and EMG signals, that are inherent in the human body channel. At present, the power consumption of filters used in IBC is relatively high. In [27], the two chips designed by Wanghao *et al.* have power consumption higher than 5 mW. Low power consumption is suggested for portable, implantable, and other application scenarios for the future development of IBC. In this work takes advantage of passive bandpass filter (BPF) to reduce system power consumption, Fig.7.

Given the differences in body impedance characteristics and the need of different transmission distances, a variable gain amplifier (VGA) is designed. A galvanic coupling method is tested on multiple volunteers by coupling a sinusoidal signal with 2 MHz frequency to the human body. The channel length was varied from 10 cm to 120 cm, and the measured signal attenuation was between 28 dB and 44dB. Therefore, a VGA with the maximum gain of 45 dB was designed, Fig. 8. The first stage amplification of the signal was performed using a VCA821 small-signal wideband amplifier. The second stage makes use of a wide-band, high-speed current feedback amplifier THS3201, suitable for ADC driving circuit with high resolution and high sampling rate due to its low distortion, high conversion rate, and strong driving ability.

F. EXPERIMENTAL PROTOCOL

The human body experimental hardware platform utilizes the XC6SLX16 device from XILINX, and the debugging environment is ISE Design Suite 14.7. Appropriate measurement setup should be provided in the experiment to separate the device grounding of the transmitter from the receiver and to avoid the coupling effect between the device grounding and the instrument. Using batteries to power the device can obtain the same results as use of a single balun at the TX site. This way can effectively isolate the internal ground of the earth-grounded equipment [28]. Battery-powered devices should be used in IBC channel test. Avoid using devices with big ground, otherwise it will lead to an optimistic estimation of channel loss [29]. To avoid the common ground of the transmitter and receiver, three ways of mutually independent peripheral circuit power supply are set up: mobile power supply (portable battery), isolation transformer power supply, and uninterrupted power supply. Among them, mobile power supply uses battery power supply, which is absolutely independent. Using isolation transformer power supply to power the device can effectively isolate the coupling between the device and the earth ground [30]. In the experiments, the uninterrupted power supply uses the storage battery to boost the voltage to provide power for the equipment, and the energy source is the battery. Tektronix THS3024 is used for waveform recording (battery-powered). When we did the human channel measurements, the power of unrelated equipment was pulled out in order to decrease the common ground interference. The power supply ways used in the experiments, which all has a small ground plane, to emulate a more realistic IBC scenario and avoid an optimistic estimation of channel loss [29]. In summary, the power supply method used in the experiment can simulate the real human communication scene.

The transmitter is connected to the volunteer's right wrist through a pair of physiological electrodes (Shanghai Cross Health Biotechnology Co., Ltd. Type: LT-1, size: 4 cm $\times$ 4 cm). The received signal is connected to the receiver through a pair of physiological electrodes and an AFE. As the distance between the transmitter and receiver electrodes increases, the two receiving electrodes move to the left arm side. In the test, the performance of the equipment under different modulation modes is tested under the motion and stationary state conditions with the channel lengths of 10, 30, 90, and 120 cm. The skin of all test subjects was cleaned with an alcoholic cotton pad at the positions of the electrodes prior to the measurements. The stationary state and motion state are described as follows: the stationary state requires volunteers to stand in front of the test bench, keep their arms extended, palms down, and stay horizontal (Fig. 9). The motion state refers to that the volunteer stands in front of the test bench, unfolds from the arm, keeps the palm downward and horizontal (initial state), and changes to the state that the arm stretches straight to the front of the body and the palm upward. The arm is bent toward the body until the upper and lower arms form a 90° angle. The arm is then allowed to move to the initial state according to the original path. Volunteers maintain a constant speed throughout the motion state, and one cycle lasts 12 s.

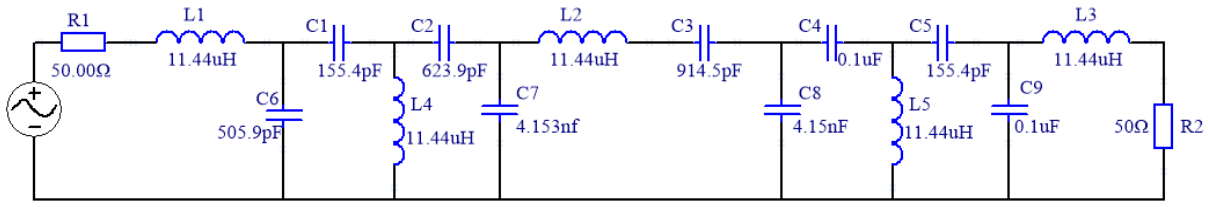

FIGURE 7. BPF circuit diagram.

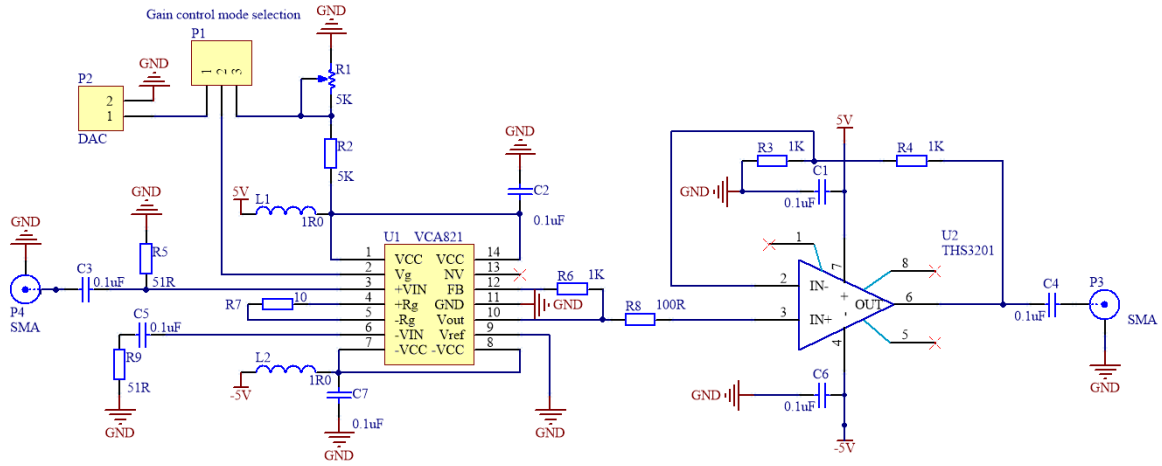

FIGURE 8. VGA circuit diagram.

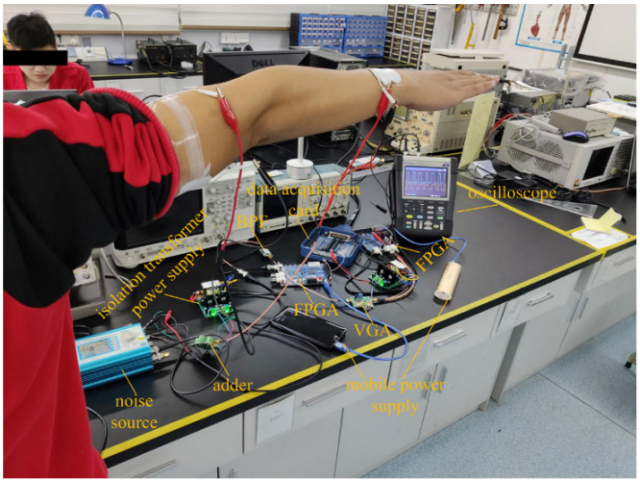

FIGURE 9. Experimental setup.

G. BER TEST PLATFORM

In order to test the BER performance, a data acquisition card (PCIe-6361, National Instruments) is used to collect the baseband data at the transmitter and the demodulated data at the receiver, Fig. 10. An XOR operation is conducted in LABVIEW, and the XOR result is collated. If the result of the XOR is not 0, then this value is regarded as an error code. Meanwhile, if the result of the XOR is 0, then this value is regarded as an accurate reception. The BER is calculated by the equation (1):

$$BER = \frac{Number\ of\ bit\ serror}{Total\ transmitted\ bits} \tag{1}$$

To increase data reliability, the amount of collected BER data meets the following requirements. The minimum amount of data to be tested needs to be greater than 1×10^7. If the BER is lower than 1×10^{-5}, then the product of the test data amount and the BER is greater than 50.

III. RESULTS AND DISCUSSIONS

A. BPF TEST AND PERFORMANCE PARAMETERS

The S_{21} and S_{11} parameters of a passive BPF are shown in Fig. 11 and are as follows: passband of -3 dB is from 1.6 MHz to 2.4 MHz. The attenuation at 500 kHz and 5 MHz is greater than 50 dB. The return loss S_{11} of the BPF is lower than -15 dB in the passband. The following will list some parameters of DSSS-DPSK galvanic coupling IBC transceiver and compared with the past researches.

Table 1 summarizes the comparison of some parameters of the past galvanic coupling IBC transceiver system with this work. In contrast, our system has the lowest coupling amplitude, which can minimize the impact of electromagnetic absorption on the human body as well as reduces the power of the transmitter to a certain extent [25]. Lower coupling amplitude and good BER performance, which is very important for low power design in practical applications.

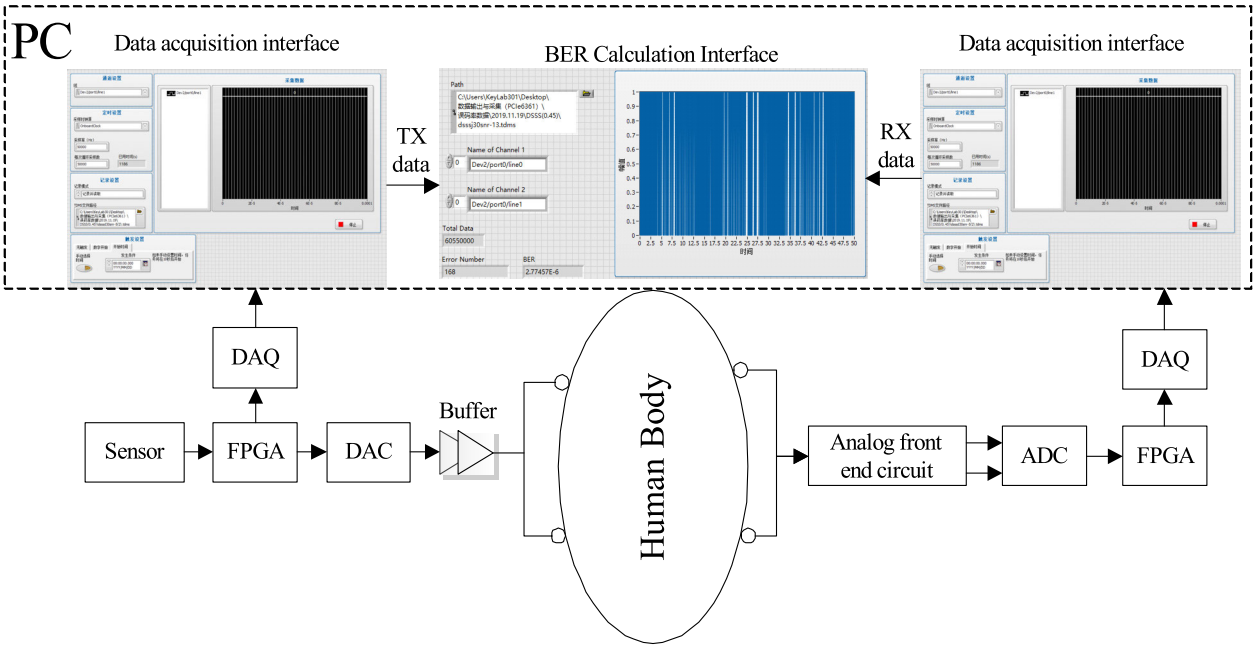

FIGURE 10. BER test platform.

TABLE 1. Comparison of some parameters of galvanic coupling IBC transceiver.

Parameters	Coupling amplitude	Carrier frequency	Modulation	Data rate
[31]	4 mA	60 kHz	CPFSK	4.8 kbps
[32], [33]	1 mA	60 kHz	BPSK	64 kbps
[23]	1 V	60 kHz	PSK	100 kbps
[25]	2.2 mA	0.1-1 MHz	OOK	1-50 kbps
Proposed work	0.392 mA	2 MHz	DSSS-DPSK	50 kbps

The following will analyze the influence of SNR, signal transmission distance, and motion status on the DSSS-DPSK and DPSK schemes. The same experimental equipment and procedures are prepared. The same environment (indoor, 20 °C ± 3 °C) and the same volunteer (i.e., male, 24 years old, 173 cm tall, 55 kg) are utilized to compare the BER of DPSK and DSSS-DPSK galvanic coupling IBC transceivers. In order to compare the BER of DPSK and DSSS-DPSK schemes, the BER of the two ought to be the same level and the coupling current of the transmitter should be reduced as much as possible. The effective value of the input current of DSSS-DPSK scheme is 0.392 mA and the one of DPSK scheme is 0.565 mA through a 15 day preliminary experiment, and the final result of this section is obtained. The current input in both experiments is lower than the safe current required in previous references [34], [35].

B. EFFECT OF SNR

Fig. 12 shows the performance of BER that varies with SNR in a channel with a length of 30 cm, with a state of motion and stationary. According to the figure, the BER shows a downward trend as SNR improves. Fig. 13 shows the average BER performance in a channel with a length of 30 cm in both motion and stationary states. Under the SNR of −20 dB, the average error rate of DSSS-DPSK and DPSK schemes in the motion and stationary state is compared. $\mathrm{BER}_{\mathrm{DPSK}(-20\ \mathrm{dB})} = 1.58 \times 10^{-1}$. $\mathrm{BER}_{\mathrm{DSSS-DPSK}(-20\ \mathrm{dB})} = 2.38 \times 10^{-3}$. After calculation, $\mathrm{BER}_{\mathrm{DPSK}(-20\ \mathrm{dB})} \div \mathrm{BER}_{\mathrm{DSSS-DPSK}(-20\ \mathrm{dB})} = 66.47 > 40$. In other SNR, the ratio of BER is also greater than 40. Therefore, under the same signal-to-noise condition, the DSSS-DPSK scheme has a BER that is much lower than that of the DPSK scheme. DSSS-DPSK schemes require lower SNR than DPSK schemes.

Fig. 13 shows the average BER performance for motion and stationary states in a certain range of SNR. According to the figure, when the BER performance changes from extremely poor (1.40×10^{-1}) to excellent (1.51×10^{-6}), the SNR of DSSS-DPSK scheme only needs to be improved by 16 dB. In contrast, when the BER performance changes from extremely poor (1.54×10^{-1}) to good (1.65×10^{-5}), the SNR of DPSK scheme needs to be improved by 25 dB. Under extremely bad conditions of the SNR of DSSS-DPSK and DPSK galvanic coupling IBC transceivers, the BER reduction of DSSS-DPSK scheme is shown to be much faster than that of DPSK when the SNR is improved. Fig. 12 shows that DPSK and DSSS-DPSK schemes are in a motion or stationary state, and the BER changes show similar rules.

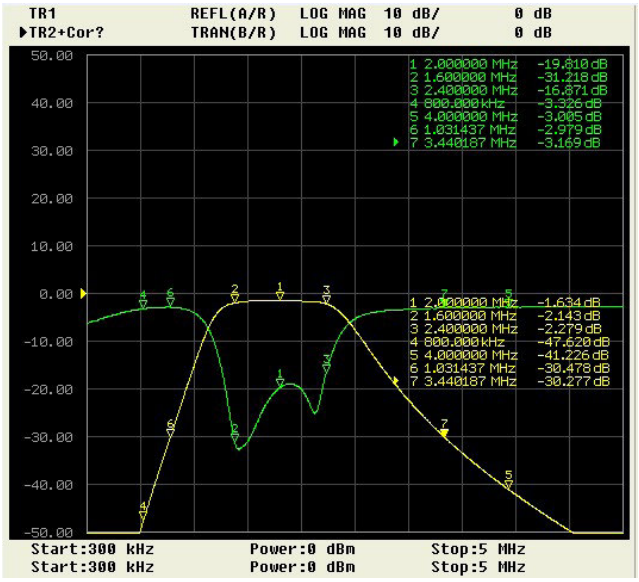

FIGURE 11. S21, S11 parameters of the BPF.

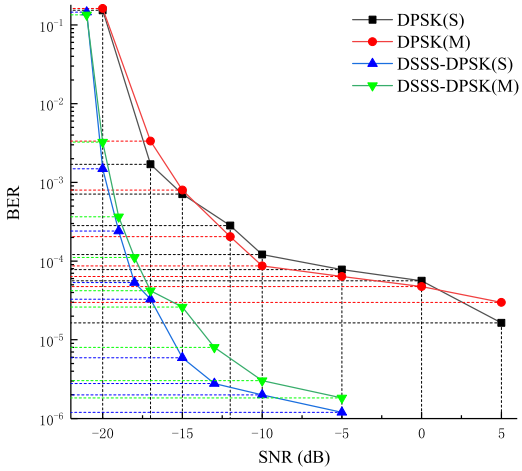

FIGURE 12. BER performances for different SNRs when the channel length is 30 cm.

The BER of DSSS-DPSK scheme is shown a sharp reduction when the SNR is improved.

C. EFFECT OF DISTANCE

Fig. 14 shows the performance of the BER as a function of channel length (10, 30, 90, and 120 cm) at SNR $= -5$ dB in both motion and stationary states. Fig. 15 shows the exponential fit performance of the average BER of motion and stationary states with the channel length at SNR $= -5$ dB. Figs. 14 and 15 show that the BER of the DSSS-DPSK and DPSK galvanic coupling IBC transceiver increases with channel length. By comparing the fitting functions of the two fitting curves in Fig. 15, the DSSS-DPSK scheme is shown to have a better BER performance than the DPSK scheme at the same channel length. In the investigated communication distance of the human body, the ratio of error rate of DPSK

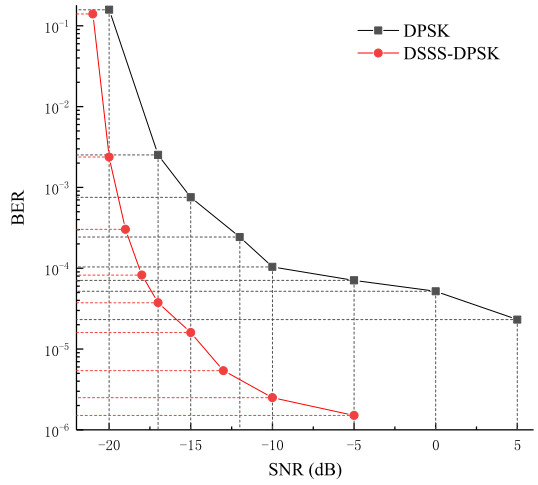

FIGURE 13. Performance of the average BER of motion and stationary state with the change in SNR.

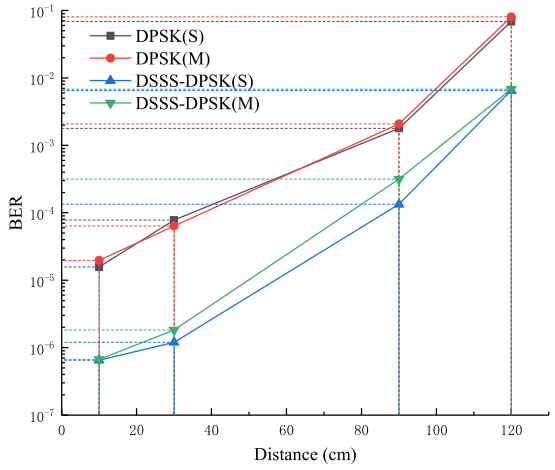

FIGURE 14. SNR performance at different distances when SNR $= -5$ dB.

to DSSS-DPSK scheme is greater than 7. The DSSS-DPSK galvanic coupling IBC transceiver's BER changes more than the DPSK's BER when the channel length is increased. However, the difference between the two devices within a limited human body channel length is not apparent. Fig. 13 reveals that DPSK and DSSS-DPSK are in a motion or stationary state, and the BER changes show similar rules.

D. EFFECT OF MOTION STATE

The statistical method is used to analyze the significant difference of data and determine whether a significant difference is found between motion and stationary state. DPSK and DSSS-DPSK schemes test results of significant differences in motion and stationary state are $P_1 = 1.01 \times 10^{-2}$, $P_2 = 9.43 \times 10^{-3}$, $P_1 < 5 \times 10^{-2}$, and $P_2 < 1 \times 10^{-2}$(Significance level $\alpha = 0.05$). The results show that the DPSK scheme has a statistically different BER performance in motion and stationary states. $P3 = 8.68 \times 10^{-4}$ and $P4 = 1.60 \times 10^{-5}$(Significance level $\alpha = 0.05$), and both values are lower

TABLE 2. Significance test of the difference between BER in motion and stationary state.

Sort	Channel length = 30 cm, Different SNR	SNR = –5 dB, Different channel length
DPSK	P_1= 1.01×10^{-2}(Remove data at SNR = –20)	P_3= 8.68×10^{-4}
DSSS-DPSK	P_2=9.43×10^{-3}(Remove data at SNR = –21)	P_4= 1.60×10^{-5}

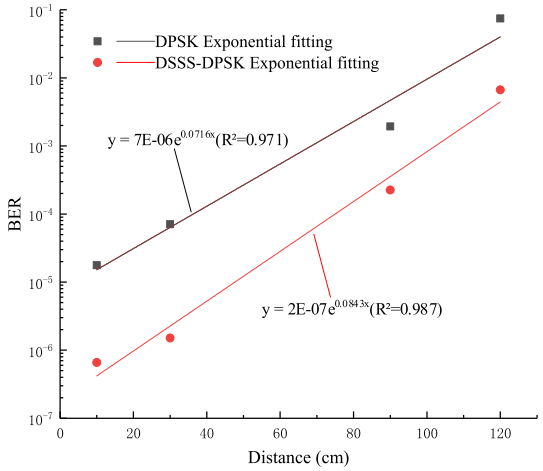

FIGURE 15. Average BER for motion and stationary states as a function of channel length.

than 1×10^{-3}. The DSSS-DPSK scheme exhibits significant statistical differences. Therefore, the DPSK and DSSS-DPSK schemes have significant statistical differences in motion and stationary state under different channel lengths, that is, BER changes when the motion state of the DSSS-DPSK and DPSK schemes varies. And the difference between DSSS-DPSK scheme motion and stationary state BER is greater than DPSK. As shown in Fig. 14, under the same SNR condition, the DSSS-DPSK scheme BER performance is better than the DPSK scheme. Therefore, it cannot be interpreted as the DSSS-DPSK scheme makes the transceiver ineffective to resistant against motion, but DSSS-DPSK scheme is more sensitive to changes in motion status than DPSK.

IV. CONCLUSION

This work uses the FPGA (XC6SLX16) as the platform and peripheral circuits to design the DSSS-DPSK and DPSK galvanic coupling IBC transceivers. Through the experiments, the variation in the BER among different SNR, different channel lengths and different motion states is compared. Results show that in both states of motion and stationary, the BER of DPSK and DSSS-DPSK schemes shows a downward trend when the SNR or channel length continues to decrease progressively. The BER of the DPSK scheme is 40 times larger than the DSSS-DPSK scheme in a channel with a length of 30 cm and different SNR experiments. When the BER performance changes from extremely poor (1.40×10^{-1}) to excellent (1.51×10^{-6}), the SNR of DSSS-DPSK scheme only needs to be improved by 16 dB. In contrast, when the BER performance changes from extremely poor (1.54×10^{-1}) to good (1.65×10^{-5}), the SNR of DPSK scheme needs to be improved by 25 dB. These findings show that the DSSS-DPSK scheme has a sharp reduction in BER when the SNR is improved. In the experiments of SNR = −5 dB with different channel lengths, the BER ratios of the DPSK scheme is 7 times larger than the DSSS-DPSK scheme. The BER changes when the motion state of the DSSS-DPSK and DPSK schemes varies. The BER performance of DSSS-DPSK scheme has a larger difference between motion and stationary state than DPSK; that is, DSSS-DPSK galvanic coupling IBC transceiver is more sensitive to changes in motion status than DPSK.

REFERENCES

[1] T. G. Zimmerman, "Personal area networks: Near-field intrabody communication," *IBM Syst. J.*, vol. 35, no. 3.4, pp. 609–617, 1996.
[2] S. Zhang, Y. Qin, J. Kuang, P. U. Mak, S. H. Pun, M. I. Vai, and Y. Liu, "Development and prospect of implantable intra-body communication technology," *J. Comput.*, vol. 9, no. 2, pp. 16–23, 2014.
[3] X. Shi and T. Zhang, "Design of a wearable fall detection device," *Chin. J. Sci.*, vol. 33, no. 3, pp. 575–580, 2012.
[4] Y. M. Gao, S. H. Pun, and M. Du, "Construction and validation of galvanic coupling human intra-body communication model with quasistatic approximation," *Space Med. Med. Eng.*, vol. 22, no. 6, pp. 427–432, 2009.
[5] A. E. Khorshid, I. N. Alquaydheb, A. M. Eltawil, and F. J. Kurdahi, "Physical multi-layer phantoms for intra-body communications," *IEEE Access*, vol. 6, pp. 42812–42821, 2018.
[6] M. S. Wegmueller, M. Oberle, N. Felber, N. Kuster, and W. Fichtner, "Signal transmission by galvanic coupling through the human body," *IEEE Trans. Instrum. Meas.*, vol. 59, no. 4, pp. 963–969, Apr. 2010.
[7] S. Zhang, S.-H. Pun, P. U. Mak, Y. P. Qin, Y. H. Liu, Y. M. Gao, and M. I. Vai, "Experimental verifications of low frequency path gain (*PG*) channel modeling for implantable medical device (IMD)," *IEEE Access*, vol. 7, pp. 11934–11945, 2019.
[8] Y.-M. Gao, Y.-T. Ye, S. Lin, Ž. L. Vasić, M.-I. Vai, M. Du, M. Cifrek, and S.-H. Pun, "Investigation of implantable signal transmission characteristics based on visible data of the human leg," *Biomed. Eng. OnLine*, vol. 16, no. 1, Dec. 2017, Art. no. 88.
[9] J. Li, Z. Nie, Y. Liu, L. Wang, and Y. Hao, "Characterization of in-body radio channels for wireless implants," *IEEE Sensors J.*, vol. 17, no. 5, pp. 1528–1537, Mar. 2017.
[10] Ž. L. Vasić, I. Krois, and M. Cifrek, "Effect of transformer symmetry on intrabody communication channel measurements using grounded instruments," *Automatika*, vol. 57, no. 1, pp. 15–26, Jan. 2016.
[11] J. Mao, H. Yang, Y. Lian, and B. Zhao, "A five-tissue-layer human body communication circuit model tunable to individual characteristics," *IEEE Trans. Biomed. Circuits Syst.*, vol. 12, no. 2, pp. 303–312, Apr. 2018.
[12] W. K. Chen and W. Z. Liu, "An investigation on phase characteristics of galvanic coupling human body communication," in *Proc. 4th Future Trends Biomed. Health Informat. Cybersecur. Med. Devices (ICBHI)*, Taiwan, Taipei, Apr. 2019, pp. 335–341.
[13] Y. Gao, S. Pan, B. Mai, M. Wei, and M. Du, "Quasi-static model and transceiver design for galvanic coupling intra-body communication," *J. Electron. Meas. Instrum.*, vol. 26, no. 8, pp. 732–737, Feb. 2013.
[14] F. Grilec, Z. L. Vasic, W. Ni, Y. Gao, M. Du, and M. Cifrek, "Wireless intrabody communication sensor node realized using PSoC microcontroller," in *Proc. 39th Int. Conv. Inf. Commun. Technol., Electron. Microelectron. (MIPRO)*, Opatija, Croatia, May 2016, pp. 426–429.

[15] H. Lee, K. Lee, S. Hong, K. Song, T. Roh, J. Bae, and H.-J. Yoo, "A 5.5 mW IEEE-802.15.6 wireless body-area-network standard transceiver for multi-channel electro-acupuncture application," in *IEEE Int. Solid-State Circuits Conf. (ISSCC) Dig. Tech. Papers*, Feb. 2013, pp. 452–453.
[16] E. Okamoto, Y. Kato, K. Seino, H. Miura, Y. Shiraishi, T. Yambe, and Y. Mitamura, "A new transcutaneous bidirectional communication for monitoring implanted artificial heart using the human body as a conductive medium," *Artif. Organs*, vol. 36, no. 10, pp. 852–858, Oct. 2012.
[17] Y.-S. Lin, C.-C. Wang, Y.-C. Liao, and S.-S. Lu, "Design and implementation of intrabody communication hub/alarm unit in IBC platform for fall prevention system," *Microw. Opt. Technol. Lett.*, vol. 56, no. 10, pp. 2345–2351, Oct. 2014.
[18] M. Seyedi, "A novel intrabody communication transceiver for biomedical applications," Ph.D. dissertation, Victoria Univ., Melbourne, VIC, Australia, 2014.
[19] Y. Song, Q. Hao, K. Zhang, M. Wang, Y. Chu, and B. Kang, "The simulation method of the galvanic coupling intrabody communication with different signal transmission paths," *IEEE Trans. Instrum. Meas.*, vol. 60, no. 4, pp. 1257–1266, Apr. 2011.
[20] D. Naranjo-Hernández, A. Callejón-Leblic, Ž. L. Vasić, M. Seyedi, and Y.-M. Gao, "Past results, present trends, and future challenges in intrabody communication," *Wireless Commun. Mobile Comput.*, vol. 2018, pp. 1–39, Mar. 2018.
[21] J. P. Zhou, *Principles of Communications*. Beijing, China: Beijing Univ. of Posts and Telecommunications Press, 2008, pp. 416–434.
[22] S. Hang Pun, Y. Ming Gao, P. Mak, M. I. Vai, and M. Du, "Quasi-static modeling of human limb for intra-body communications with experiments," *IEEE Trans. Inf. Technol. Biomed.*, vol. 15, no. 6, pp. 870–876, Nov. 2011.
[23] X. Chen, P. Mak, S. Pun, Y. Gao, C.-T. Lam, M. Vai, and M. Du, "Study of channel characteristics for galvanic-type intra-body communication based on a transfer function from a quasi-static field model," *Sensors*, vol. 12, no. 12, pp. 16433–16450, 2012.
[24] C. X. Fan, *Principles of Communications*. Beijing, China: National Defense Industry Press, 2012, pp. 179–199.
[25] W. J. Tomlinson, S. Banou, S. Blechinger-Slocum, C. Yu, and K. R. Chowdhury, "Body-guided galvanic coupling communication for secure biometric data," *IEEE Trans. Wireless Commun.*, vol. 18, no. 8, pp. 4143–4156, Aug. 2019.
[26] J. P. Costas, "Synchronous communications," *Proc. Inst. Radio Eng.*, vol. 12, no. 12, pp. 16433–16450, 2012.
[27] H. Wang, X. Tang, C. S. Choy, K. N. Leung, and K. P. Pun, "A 5.4-mW 180-cm transmission distance 2.5-Mb/s advanced techniques-based novel intrabody communication receiver analog front end," *IEEE Trans. Very Large Scale Integr. (VLSI) Syst.*, vol. 23, no. 12, pp. 2829–2841, Dec. 2015.
[28] M. A. Callejon, J. Reina-Tosina, D. Naranjo-Hernandez, and L. M. Roa, "Measurement issues in galvanic intrabody communication: Influence of experimental setup," *IEEE Trans. Biomed. Eng.*, vol. 62, no. 11, pp. 2724–2732, Nov. 2015.
[29] S. Maity, M. He, M. Nath, D. Das, B. Chatterjee, and S. Sen, "Bio-physical modeling, characterization, and optimization of electro-quasistatic human body communication," *IEEE Trans. Biomed. Eng.*, vol. 66, no. 6, pp. 1791–1802, Jun. 2019.
[30] N. Spina, V. Fiore, P. Lombardo, E. Ragonese, and G. Palmisano, "Current-reuse transformer-coupled oscillators with output power combining for galvanically isolated power transfer systems," *IEEE Trans. Circuits Syst. I, Reg. Papers*, vol. 62, no. 12, pp. 2940–2948, Dec. 2015.
[31] M. Oberle, "Low power system-on-chip for biomedical application," Ph.D. dissertation, ETH Zurich, Zurich, Switzerland, 2002.
[32] M. S. Wegmueller, M. Oberle, N. Felber, N. Kuster, and W. Fichtner, "Digital data communication through the human body for biomedical monitoring sensor," in *Proc. World Congr. Med. Phys. Biomed. Eng.*, Seoul, South Korea, 2006, pp. 608–612.
[33] M. S. Wegmueller, M. Oberle, N. Felber, N. Kuster, and W. Fichtner, "Signal transmission by galvanic coupling through the human body," *IEEE Trans. Instrum. Meas.*, vol. 59, no. 4, pp. 963–969, Apr. 2010.
[34] S. Lin, Y.-M. Gao, J. Cai, Ž. L. Vasić, M.-I. Vai, M. Du, M. Cifrek, and S.-H. Pun, "Biological evaluation of the effect of galvanic coupling intra-body communication on human skin fibroblast cells," *Wireless Commun. Mobile Comput.*, vol. 2017, pp. 1–8, Sep. 2017.
[35] Y.-M. Gao, H.-F. Zhang, S. Lin, R.-X. Jiang, Z.-Y. Chen, Ž. L. Vasić, M.-I. Vai, M. Du, M. Cifrek, and S.-H. Pun, "Electrical exposure analysis of galvanic-coupled intra-body communication based on the empirical arm models," *Biomed. Eng. OnLine*, vol. 17, no. 1, Dec. 2018, Art. no. 71.

W. K. CHEN received the B.S. degree from the College of Information Engineering, Northeast Electric Power University, Jilin, China, in 2017. He is currently pursuing the M.S. degree from the College of Physical and Information Engineering, Fuzhou University. His current research interests include intra-body communication and biomedical signal detecting technology.

Z. L. WEI received the B.S. degree from the College of Information Science and Engineering, Huaqiao University, Xiamen, China, in 2018. He is currently pursuing the M.S. degree with the College of Physical and Information Engineering, Fuzhou University. His current research interests include intra-body communication, biomedical signal acquisition, and electrical impedance myography.

Y. M. GAO received the Ph.D. degree in electrical engineering from Fuzhou University, Fuzhou, China, in 2010. Since 2004, he has been involved in research in the areas of bioelectromagnetism and biomedical signal detecting technology. He is currently a Professor with the College of Physical and Information Engineering, Fuzhou University.

Ž. LUČEV VASIĆ (Member, IEEE) received the Dipl.lng. and Ph.D. degrees in electrical engineering from the University of Zagreb, Zagreb, Croatia, in 2007 and 2014, respectively. She is currently an Assistant Professor with the Department of Electronic Systems and Information Processing, Faculty of Electrical Engineering and Computing, University of Zagreb. Her research activities are in the field of biomedical electronic instrumentation and human-body signal transmission. She is a member of IFMBE and CROMBES. She serves as the Vice-President of the IEEE EMB Croatian section.

M. CIFREK (Member, IEEE) received the Dipl.Ing., M.Sc., and Ph.D. degrees in electrical engineering from the Faculty of Electrical Engineering and Computing, University of Zagreb, Zagreb, Croatia, in 1987, 1992, and 1997, respectively, all in electrical engineering. He is currently a Professor of electrical engineering with the Department of Electronic Systems and Information Processing, Faculty of Electrical Engineering and Computing, University of Zagreb. His research interests are focused on the design of biomedical instrumentation and biomedical signal analysis for research and clinical applications. He is a member of IFMBE, CROMBES, KoREMA, and HMD. Since 2005, he has been a member of the Croatian Academy of Engineering.

M. I. VAI (Senior Member, IEEE) received the Ph.D. degree in electrical and electronics engineering from the University of Macau, SAR, China, in 2002. Since 1984, he has been performing research in the areas of digital signal processing and embedded systems. He is currently the Co-Ordinator of the State Key Laboratory of Analog and Mixed-Signal VLSI and an Associate Professor of electrical and computer engineering with the Faculty of Science and Technology, University of Macau.

M. DU received the Ph.D. degree in electrical engineering from Fuzhou University, Fuzhou, China, in 2005. Since 2007, she has been the Associate Director of the Key Laboratory of Eco-Industrial Green Technology of Fujian Province, Nanping, China. She is currently a Professor and a Ph.D. Supervisor with Fuzhou University. Her research interests include smart instrument and photoelectric.

S. H. PUN received the M.S. degree in computer and electrical program from the University of Porto, Portugal, in 1999, and the Ph.D. degree in the electrical and electronics engineering from the University of Macau, Macau, in 2012. He is currently an Associate Professor with the State Key Laboratory of Analog and Mixed-Signal VLSI, University of Macau. His current research interests include biomedical electronic circuits, miniaturized sensors for biomedical applications, and human-body communication.